Synthesis and characterization of potent inhibitors of Trypanosoma cruzi dihydrofolate reductase

9 AUTHORS, INCLUDING:

Norbert Schormann
University of Alabama at Birmingham
37 PUBLICATIONS **397** CITATIONS

Sadanandan E Velu
University of Alabama at Birmingham
74 PUBLICATIONS **673** CITATIONS

Bidhan A Shinkre
Syngene International Ltd.
19 PUBLICATIONS **338** CITATIONS

Debasish Chattopadhyay
University of Alabama at Birmingham
62 PUBLICATIONS **907** CITATIONS

Synthesis and characterization of potent inhibitors of *Trypanosoma cruzi* dihydrofolate reductase

Norbert Schormann [a], Sadanandan E. Velu [b], Srinivasan Murugesan [b], Olga Senkovich [a], Kiera Walker [a], Bala C. Chenna [b], Bidhan Shinkre [b], Amar Desai [a], Debasish Chattopadhyay [a,*]

[a] *Department of Medicine and Center for Biophysical Sciences and Engineering, University of Alabama at Birmingham, Birmingham, AL 35294, USA*
[b] *Department of Chemistry, University of Alabama at Birmingham, Birmingham, AL 35294, USA*

ARTICLE INFO

ABSTRACT

Dihydrofolate reductase (DHFR) of the parasite *Trypanosoma cruzi* (*T. cruzi*) is a potential target for developing drugs to treat Chagas' disease. We have undertaken a detailed structure–activity study of this enzyme. We report here synthesis and characterization of six potent inhibitors of the parasitic enzyme. Inhibitory activity of each compound was determined against *T. cruzi* and human DHFR. One of these compounds, ethyl 4-(5-[(2,4-diamino-6-quinazolinyl)methyl]amino-2-methoxyphenoxy)butanoate (**6b**) was co-crystallized with the bifunctional dihydrofolate reductase-thymidylate synthase enzyme of *T. cruzi* and the crystal structure of the ternary enzyme:cofactor:inhibitor complex was determined. Molecular docking was used to analyze the potential interactions of all inhibitors with *T. cruzi* DHFR and human DHFR. Inhibitory activities of these compounds are discussed in the light of enzyme–ligand interactions. Binding affinities of each inhibitor for the respective enzymes were calculated based on the experimental or docked binding mode. An estimated 60–70% of the total binding energy is contributed by the 2,4-diaminoquinazoline scaffold.

1. Introduction

Chagas' disease is caused by the protozoan parasite *Trypanosoma cruzi*, which is primarily transmitted by an insect vector but also via blood transfusion, organ transplant, and from mother to child. The disease affects millions of people in Latin America where the vector and the parasite are endemic.[1] Nevertheless, since the infected hosts, if untreated can carry the parasite through their life increased travel and immigration give rise to an emerging threat in many countries outside the endemic regions. But the drugs used for the treatment of *T. cruzi* infection cause serious side effects and are not effective in the chronic stage of the disease. Therefore, validating potential drug targets and identifying novel drug candidates is of considerable global importance. Since the dihydrofolate reductase (DHFR) activity of *T. cruzi* (*Tc*DHFR) is essential for the parasite, it represents a potential target for rational drug design. DHFR has a proven track record as a drug target in cancer chemotherapy. More importantly, DHFR inhibitors are successfully used in the treatment of bacterial and parasitic infections.[2–5] While DHFR is a monofunctional protein in mammals, *T. cruzi* and other protozoan parasites carry a bifunctional form of the enzyme in which the DHFR domain is linked to the thymidylate synthase (TS) domain with a linker sequence whose length varies from one parasite to the other. Earlier data from our laboratory showed that an inhibitor of *Tc*DHFR, namely the antifolate drug trimetrexate (TMQ), inhibits the growth of amastigote and trypomastigote forms of *T. cruzi* in vitro.[6] However, very few, if any, high affinity inhibitors of *Tc*DHFR have been reported. In order to facilitate rational design of a selective inhibitor of the *T. cruzi* enzyme we have initiated a comprehensive structure–activity study using various antifolate molecules through selective library search and limited chemical synthesis. As part of this study we previously characterized the structure of the biologically relevant bifunctional form of the parasitic enzyme, (*Tc*DHFR–TS), and determined the structure of the enzyme with TMQ bound to the DHFR active site.[7] We also identified a number of highly active inhibitors of *Tc*DHFR from libraries of antifolate compounds and developed a three-dimensional model for quantitative structure–activity (3D-QSAR) analysis of inhibitors of *Tc*DHFR activity.[8]

Based on earlier results of Davoll et al.[9] and our data we have recently synthesized six compounds that contain the 2,4-diaminoquinazoline scaffold similar to TMQ but the methyl group at the C5-position in the quinazoline ring is absent (Fig. 1). Moreover, structural modifications were made to the phenyl ring and the linker nitrogen atom of TMQ. We report here the synthesis and characterization of these compounds and their inhibitory activity against TcDHFR and human DHFR. In order to determine the binding mode of the synthesized compounds in the enzyme active site, we co-crystallized one inhibitor, ethyl 4-(5-[(2,4-diamino-6-quinazolinyl)methyl]amino-2-methoxyphenoxy)butanoate (6b) with the T. cruzi bifunctional enzyme and NADPH and determined the structure of the ternary complex. We used molecular docking to predict the binding of all inhibitors in T. cruzi and human DHFR (hDHFR). The binding poses were used in the calculation of binding affinities of these inhibitors for both enzymes. Experimentally determined enzyme inhibition data are explained in the light of these calculations. Throughout the work, we used a recombinant preparation of bifunctional TcDHFR–TS enzyme for enzyme inhibition assays and structural studies.

2. Results and discussion

All organisms require folate. Reduced forms of folate and its derivatives are necessary for synthesis of essential biomolecules such as protein, DNA, and RNA. As a result, metabolic steps leading to the biosynthesis and modification of folates have been extensively studied and enzymes involved in these pathways have been targets of many clinically used drugs. Among these enzymes, DHFR, in addition to being one of the most common targets for cancer chemotherapy, has been exceptionally successful as a target for antibacterial and antiparasitic agents. This is remarkable considering that DHFR is an evolutionarily conserved enzyme and many residues involved in the reaction mechanism and substrate binding are also highly conserved among various organisms. Since DHFR is an essential enzyme in humans, any cross-reactivity with hDHFR renders the drugs toxic to the host. Nevertheless, certain drugs show high degree of selectivity towards DHFR of different pathogens as compared to the human enzyme. Therefore, it is conceivable that a therapeutically useful inhibitor of TcDHFR may be developed. However, as Gilbert[10] noted in his review on inhibitors of leishmanial and trypanosomal DHFRs, reports of such inhibitors have been limited. Nevertheless, results of limited medicinal chemistry as well as in silico docking efforts reiterate the promise

of this enzyme for developing drugs against Chagas' disease and underscore the need for further investigation.[11–13]

TMQ is an excellent inhibitor of TcDHFR and is highly effective in inhibiting growth of T. cruzi in vitro in tissue culture. However, TMQ, despite being an FDA approved drug (for treatment of Pneumocystis carinii infection in AIDS patients), suffers from serious limitations. TMQ is also a potent inhibitor of hDHFR and therefore requires co-administration with leukovorin in order to rescue the host cells from the toxic effect of the drug. However, the potent activity of TMQ against the parasite combined with previous studies indicating antiparasitic activity of 2,4-diaminoquinazoline antifolates emphasizes the importance of further structure–activity studies on this class of compounds. We have now synthesized six compounds that retain the 2,4-diaminoquinazoline scaffold but contain modifications in the phenyl ring and the N-linker (Fig. 1) to examine if new contacts with the parasitic enzyme, especially near the active site residue Met49, can be achieved. Since the corresponding residue in hDHFR is Phe31, we hoped that the modifications may have adverse effect on the binding of these compounds in hDHFR.

2.1. Enzyme inhibition

All six compounds reported here are potent inhibitors of TcDHFR with IC_{50} values in the nanomolar range. Inhibitory activities against TcDHFR and hDHFR are summarized in Table 1. We determined experimental K_i values for 6a and 6b using Lineweaver–Burk plots (Fig. 2). These values agree well with the K_i values calculated from the average IC_{50} values. However, all compounds show excellent inhibition of hDHFR, although the IC_{50} values are three to sixfold higher. As a consequence, the selectivity indices of these inhibitors are comparable to that of TMQ (SI = 4).

2.2. Crystal structure

In an attempt to analyze the effect of modifications on the binding of the inhibitors within the enzyme active site, we determined the structure of the ternary enzyme:cofactor:inhibitor complex using one of the inhibitors, namely 6b. The bifunctional TcDHFR–TS enzyme was used in crystallization. The structure of this complex was refined to a resolution of 2.5 Å (R of 20.0%, R_{free} of 23.4%; see Table 2). The asymmetric unit contains four TcDHFR–TS subunits (A, B, C and D) with one cofactor (NADP) and the inhibitor 6b bound to each DHFR domain and one sulfate ion at the phosphate binding site in each TS domain. In addition to the
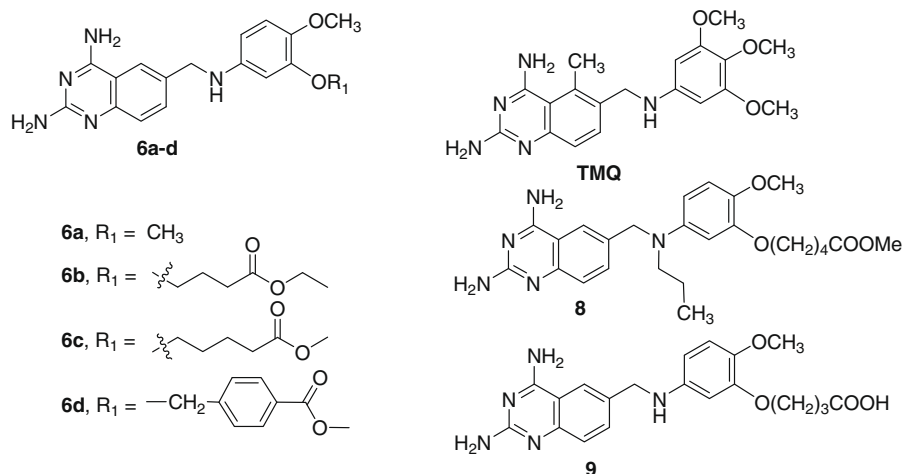

Figure 1. Target structures of the synthesized analogs.

Table 1a
Inhibitory activity against TcDHFR and hDHFR

	TcDHFR		hDHFR		SI (IC_{50})	SI (K_i)
	IC_{50} (nM)	K_i (nM)	IC_{50} (nM)	K_i (nM)		
6a	27.1 ± 4.7	1.6 ± 0.4	85.5 ± 11.2	11.8 ± 0.8	3.2	7.4
6b	23.8 ± 7.0	1.3 ± 0.2	68.3 ± 5.6	9.6 ± 1.5	2.9	7.4
6c	27.0 ± 4.0	1.6 ± 0.2	93.5 ± 10.8	13.0 ± 1.6	3.5	8.1
6d	57.5 ± 4.6	3.3 ± 0.6	174.6 ± 15.2	24.5 ± 4.3	3.0	7.4
8	422 ± 64	24.9 ± 6.4	1338 ± 167	188 ± 32	3.2	7.6
9	61.0 ± 6.6	3.6 ± 0.8	356.6 ± 28.1	49.8 ± 7.0	5.8	13.8
TMQ[a]	20.2 ± 6.6	6.6 ± 0.6		80.9 ± 12.5	4.0	

$IC_{50} = c_i/(v_o/v_i - 1)$ and $K_i = IC_{50}/(S/K_m + 1)$[b]
K_i calculation uses the Michaelis–Menten equation for competitive inhibition: for $S \gg K_m$, $K_i \ll IC_{50}$
SI (selectivity index) defined as IC_{50} (hDHFR)/IC_{50} (TcDHFR) or K_i (hDHFR)/K_i (TcDHFR)

[a] Experimental activity data for TMQ are taken from Ref. 6.
[b] K_m (DHF) values used for calculation of K_i are 1.2 and 2.8 µM for TcDHFR and hDHFR, and were taken from Refs. 28,29, respectively.

Table 1b
Experimental K_i for compounds **6a** and **6b**.

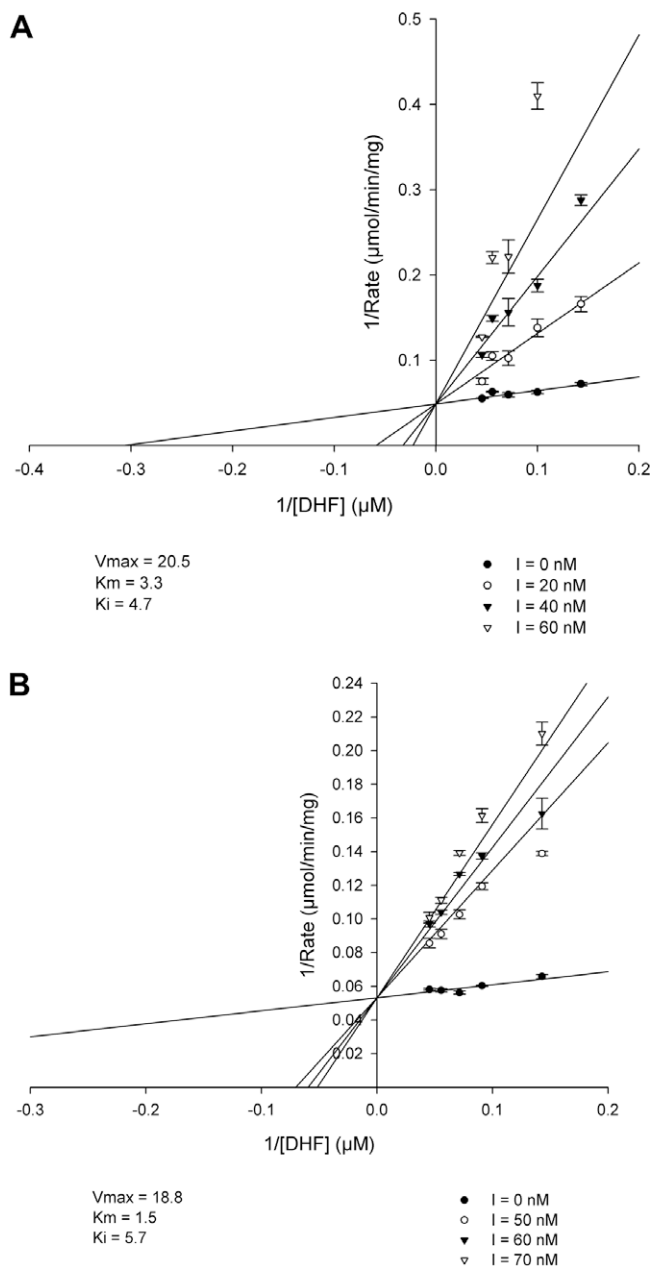| |
|---|
| **6a**: K_i = 4.75 ± 0.98 nM (K_m = 3.25 ± 0.82 nM; R^2 = 0.990) |
| **6b**: K_i = 5.68 ± 1.13 nM (K_m = 1.45 ± 0.32 nM; R^2 = 0.998) |

C-terminal 6 or 7 residues several residues in a loop region (residue number 110–121) are missing in each subunit. The final model contains 99.8% of all protein residues in the allowed regions of the Ramachandran plot. Quality of electron density for placing the inhibitor was excellent except for the ethylbutanoate chain (Fig. 3). Several atoms of this chain were disordered in all four subunits. Electron density for the NADP molecule was also of excellent quality.

Overall structure of the protein in this complex is very similar to structures described earlier for inhibitor-free TcDHFR–TS and the TMQ complex. No major change in the protein structure is noticed in the DHFR domain upon binding of the inhibitor except some movement of the Met49 side chain. The inhibitor is bound in the hydrophobic pocket with the pyrimidine ring of the 2,4-diaminoquinazoline scaffold stacked against residue Phe52. The cofactor molecule is involved in extensive interactions with the enzyme but provides only weak stacking interaction with the quinazoline ring of the inhibitor. Ternary (enzyme:cofactor:inhibitor) complexes of DHFRs with both the oxidized and reduced forms of the cofactor have been reported suggesting that the oxidation state of the cofactor may not determine inhibitor binding.[7,14] Carboxyl oxygen atoms of the side chain of Asp48 and the main chain O atom of Val26 provide major hydrophilic interactions for the inhibitor. As predicted, the ethylbutanoate chain packs against residue Met49. Also, the methoxy group of the inhibitor makes a hydrophobic interaction with the methyl group of Met49 side chain (Fig. 4).

There was one unexplained density in a pocket near the interface of the DHFR and TS domains in each subunit. In the crystal structures of TcDHFR–TS reported earlier, sulfate ions or ethylene glycol molecules were placed in this region. However, attempts to refine sulfate ions or ethylene glycol in the present structure were unsuccessful and resulted in ambiguous density and unreasonable temperature factors. Moreover, Cys403 in the TS domain seems to have been modified at least in the A subunit, although the nature of the modification could not be resolved at this time.

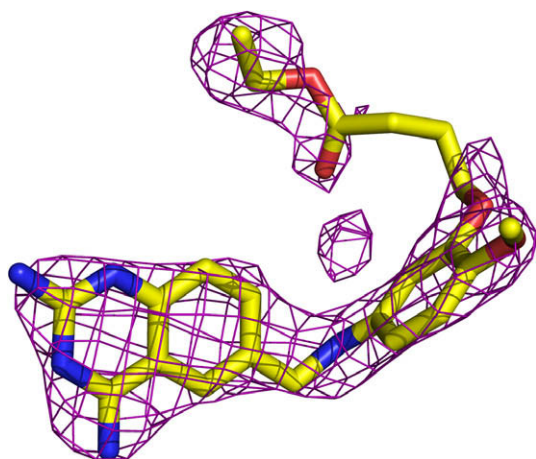## 2.3. Docking and binding affinity

We used molecular docking for further analysis of the results. The experimental binding modes of TMQ (PDBID: 3HBB) and **6b** (PDBID: 3KJS) provide a framework for predicting binding modes

Vmax = 20.5
Km = 3.3
Ki = 4.7

● I = 0 nM
○ I = 20 nM
▼ I = 40 nM
▽ I = 60 nM

Vmax = 18.8
Km = 1.5
Ki = 5.7

● I = 0 nM
○ I = 50 nM
▼ I = 60 nM
▽ I = 70 nM

Figure 2. Lineweaver–Burk plots. (A) Compound **6a**. (B) Compound **6b**.

Table 2
Crystal data, data collection, and refinement statistics for TcDHFR–TS:**6b** complex

Crystal data	
Space group	P4$_3$2$_1$2
Unit cell parameters (Å)	a = 175.93, b = 175.93, c = 250.35
Resolution range (Å)	19.99–2.50 (2.59–2.50)*
Redundancy	4.0 (3.6)
Completeness (%)	99.6 (98.9)
R_{merge} (%)	6.0 (25.6)
I/σ	13.0 (4.0)
Refinement statistics	
Resolution (Å)	19.99–2.50 (2.56–2.50)
No. of reflections	126968 (9574)
Completeness (%)	99.6 (99.7)
R_{all} (%)	20.2
R_{work} (%)	20.0 (27.0)
R_{free} (%)	23.4 (30.9)
No. of atoms	
Total	17053
Protein	15908
Ligand	316
Ethylene glycol	52
Ion	40
Water	737
Wilson B-factor (Å^2)	35.3
Average B-factors (Å^2)	
Overall	28.7
Protein	28.2
Ligand (inhibitor + NADPH)	44.8
Ethylene glycol	56.1
Ion	81.4
Water	28.3
R.m.s. deviations	
Bonds (Å)	0.007
Angles (°)	1.18
Coordinate error ESU	0.15
Correlation coefficient	
F_oF_c	0.95
F_oF_c free	0.93
Ramachandran plot	
Allowed (%)	99.8
Disallowed (%)	0.2 [1 residue per subunit]

* Numbers in parentheses represent highest resolution shell.

Figure 3. Electron density map ($F_o - F_c$, contoured at 3.0σ) for compound **6b**.

Figure 4. Location of inhibitor **6b** in the active site of TcDHFR. Inhibitor molecule **6b** is shown as stick model (color code: yellow-C, blue-N, red-C); protein residues are in surface representation with selected labeled residues (Val26, Asp48, and Met49) as stick models (color code: white-C, blue-N, and red-O). Hydrophobic interactions between the inhibitor molecule and side chain atoms of Met49 are also shown.

and amino groups in the 2,4-diaminoquinazoline ring and the backbone O atoms of residues Val26, Val27, and Ile154 as well as the side chain O atoms of Asp48 in the TcDHFR active site. A similar hydrogen bonding pattern is observed for the remaining five compounds with the differences being attributed to the degree of superimposition of the 2,4-diaminoquinazoline scaffolds.

Docked poses of the inhibitors in the TcDHFR binding pocket (Fig. 5A) reveal that the introduced modifications do not involve additional interactions with the protein except enhanced hydrophobic interaction with Met49 for some inhibitors. Rather most inhibitors extend into an open area of the protein structure. Inherent flexibility in the structure of DHFRs has been described particularly in studies on *Escherichia coli* DHFR.[15,16] These studies showed that during transition between different states of the enzyme the largest conformational change occurs in the Met20 loop of DHFR (corresponds to Ile41 loop in *T. cruzi* DHFR) and is accompanied by the motion of the cofactor into and out of the binding pocket. Conformational changes involving ligand (substrate or inhibitor) and cofactor binding play important roles in determining the functional outcome for enzyme catalysis and inhibitor activity.[17] In our studies with various inhibitors of TcDHFR, we noticed movement in the protein structure.[8] Flexibility in the target active site makes it possible for even large substituent groups to pack in the open space as shown in the close up views of **6b** and **6d** in the pocket (Fig. 5B and C). In the crystal structure of the enzyme-inhibitor complex, part of the ethylbutanoate ester chain of **6b** shows no interaction with the protein or solvent and remains disordered (Fig. 3). On the other hand, this structure suggests that the Phe88 residue in TcDHFR may be targeted for selective hydrophobic interaction since the amino acid residue in the equivalent position in hDHFR is Asn64 (Fig. 6).

The binding (docking) modes of all compounds in the hDHFR active site are shown in Figure 7A. The docked pose of CO4 for which a co-crystal structure with hDHFR is available was used as a guide to compare the reliability of the docked conformations.[18] The 2,4-diaminoquinazoline moiety of the inhibitors packs tightly in the hDHFR active site providing major binding interactions. The quinazoline ring stacks against the phenyl ring of residue Phe32. As in TcDHFR active site, the inhibitors extend to the open solvent exposed region of the molecule. If the inhibitors would have adopted the same conformation in the active sites of both TcDHFR and hDHFR, several inhibitors would be expected to clash in hDHFR

of the remaining compounds using molecular docking. Previously, we showed that the docking poses quite accurately capture the binding mode in the crystal structure with *r.m.s.* deviations of 1.17 and 1.53 Å between the X-ray pose and docking pose for TMQ and **6b**, respectively.[8] The calculated total estimated ligand–receptor interaction energy and the hydrogen bonding pattern are essentially the same for both poses of each molecule (see Table 3). Hydrogen bonds are observed between ring N-atoms

Table 3
Estimated binding affinities based on docked poses of inhibitors within TcDHFR and hDHFR active site

	ΔG (kcal mol^{-1})	MW	N_{heavy}[a]	LE[b]	K_d (nM)	$-\log K_d$
TcDHFR						
6a	−12.07	325	24	0.50	1.8	8.74
6b	−11.92 (−11.58)[c]	425	31	0.38 (0.37)	2.4 (4.2)	8.62 (8.38)
6c	−12.43	397	29	0.43	1.0	9.00
6d	−12.21	459	34	0.36	1.5	8.84
8	−8.36	468	34	0.25	889	6.05
9	−9.13	425	31	0.29	246	6.61
TMQ	−10.09 (−9.72)	369	27	0.37 (0.36)	50 (92)	7.30 (7.04)
hDHFR						
6a	−11.32	325	24	0.47	6.4	8.19
6b	−13.33	425	31	0.43	0.2	9.65
6c	−12.55	397	29	0.43	0.8	9.08
6d	−11.59	459	34	0.34	4.1	8.39
8	−12.92	468	34	0.38	0.4	9.35
9	−13.48	425	31	0.43	0.2	9.76
CO4	−13.52 (−11.71)	384	28	0.48 (0.42)	0.2 (3.3)	9.79 (8.48)

	TcDHFR			hDHFR		
	ΔG [kcal mol^{-1}]	LE[d]	K_i [nM]	ΔG [kcal mol^{-1}]	LE[d]	K_i [nM]
6a	−12.15	0.51	1.6	−10.95	0.46	11.8
6b	−12.28	0.40	1.3	−11.08	0.36	9.6
6c	−12.15	0.42	1.6	−10.89	0.38	13.0
6d	−11.72	0.34	3.3	−10.51	0.31	24.5
8	−10.51	0.31	24.9	−9.29	0.27	188
9	−11.67	0.38	3.6	−10.09	0.33	49.8
TMQ	−11.30	0.42	6.6			

Based on results from PEARLS web server (http://ang.cz3.nus.edu.sg/cgi-bin/prog/rune.pl).[26]
$\Delta G = -RT \ln K_d$ (RT ∼ 0.6 kcal mol^{-1} for T = 298 K).
[a] N_{heavy} = Non-hydrogen atoms.
[b] LE = $\Delta G/N_{heavy}$ (ligand efficiency) [based on affinity in docked poses; K_d].
[c] Values based on X-ray crystal structures are shown within parenthesis.
[d] LE = $\Delta G/N_{heavy}$ (ligand efficiency) [based on activity; K_i].
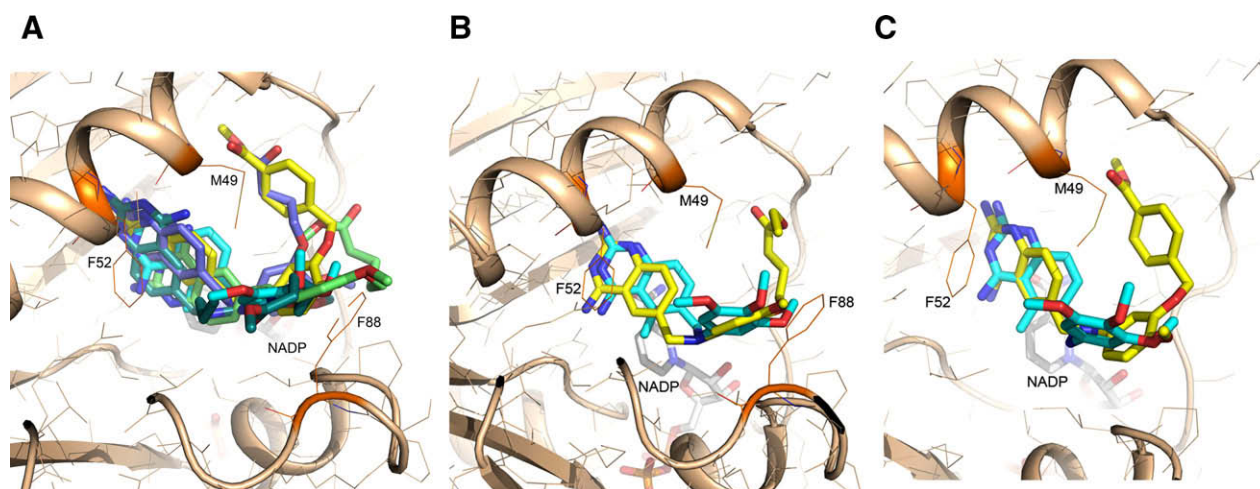
Figure 5. Docking of the inhibitors into the active site of TcDHFR. (A) Docked poses of inhibitors in TcDHFR active site. Protein structure is shown as a cartoon diagram, ligands, and NADP are shown as stick models with selected residues (Met49, Phe52, Phe88) shown in line representation. (B) Docked pose of compound **6b** is shown in yellow (C), red (O), and blue (N). For comparison TMQ is also shown as stick model (color code: cyan-C, red-O, blue-N). Residues Met49, Phe52, and Phe88 are shown in line representation and are labeled. (C) Docked pose of compound **6d** shown in yellow (C), red (O), and blue (N). For comparison TMQ is also shown as stick model (color code: cyan-C, red-O, blue-N). Protein residues Met49 and Phe52 shown in line representation are labeled.

in particular with Leu22 (Fig. 7B). Instead, both the inhibitor and protein residues undergo conformational changes. In addition, the side chain amino group of Gln35 in hDHFR is positioned within hydrogen bonding distance from acceptor oxygen atoms of several inhibitors, thereby enhancing the affinity of these inhibitors for hDHFR and resulting in a decrease in selectivity (Fig. 7C).

We calculated the binding affinity of each inhibitor for TcDHFR and hDHFR based on their docking poses in the respective en-

zyme's active site (Table 3). For comparison, we also estimated binding affinities of TMQ and **6b** for TcDHFR based on the crystal structures of these inhibitors with TcDHFR–TS and the binding affinity of CO4 based on its crystal structure with hDHFR. As shown in Table 4, energy analysis of binding for these lipophilic inhibitors demonstrates that the van der Waals energy portion provides the main contribution to the total energy of binding. The contribution of hydrogen bonding energy to the total energy varies between 5%
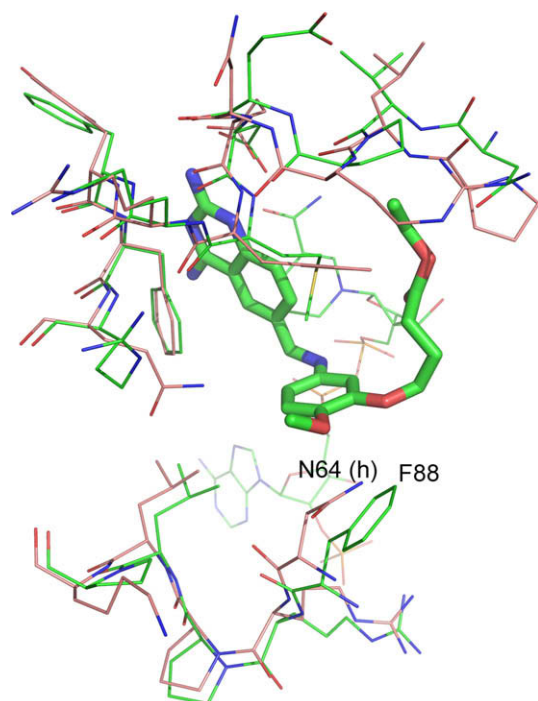
Figure 6. Superimposition of active sites in *Tc*DHFR and hDHFR. Crystal structure of *Tc*DHFR domain (residues 20–232) in the ternary complex of *Tc*DHFRTS:NADP:**6b** was superimposed on the crystal structure of hDHFR in the CO4 complex. Protein residues are shown in line representation. Color code for *Tc*DHFR: green (C), blue (N), red (O); color code for hDHFR: rose (C), blue (N), red (O). Inhibitor **6b** is shown as stick model with the same color code as *Tc*DHFR. Location of one of the dissimilar residues near the active site (Phe88 in *Tc*DHFR and Asn64 in hDHFR) is labeled.

and 20% among these compounds. The 2,4-diaminoquinazoline scaffold provides 60–70% of the total ligand-receptor binding energy (∼70% of the total van der Waals energy and 80–100% of the total hydrogen bond energy for each inhibitor). We also calculated the ligand efficiency (LE) of the six inhibitors for *Tc*DHFR and hDHFR based on experimental activities and estimated binding affinities. Ligand efficiency is defined as the free energy contribution per 'heavy atom'. The formula '$\Delta G = -RT\ln K$' correlates the free energy of binding with either the inhibitory activity (K_i) or the binding affinity (K_d). Although activities and binding affinities for enzyme inhibitors are defined differently, we observe a very good correlation between LE values based on experimental inhibitory activities and estimated affinities of inhibitors **6a–d** and TMQ for *Tc*DHFR, while the correlation for inhibitors **8** and **9** is not good (values of K_i and K_d differ 36–68-fold, see Table 3). In the case of hDHFR we only observe a good correlation for inhibitors **6a** and **6c** (Table 3).

3. Conclusion

The synthesized molecules are potent inhibitors of *T. cruzi* DHFR activity. However, these compounds also show high degree of inhibitory activity against the human enzyme. Introduced chemical modifications were not effective in either providing sufficient additional favorable contacts with the parasitic enzyme or unfavorable contacts with the host protein. Some of the substituent groups showed hydrophobic interactions with Met49 of *Tc*DHFR. However, these interactions did not provide a net gain in selectivity. The 2,4-diaminoquinazoline scaffold makes a large contribution towards the energy of binding of these molecules in the active sites of both enzymes. Moreover, flexibility in the structure of the DHFR active site allows binding of even very large inhibitors

without significant clashes. Therefore, modifications outside the 2,4-diaminoquinazoline scaffold were not effective in enhancing selectivity for the parasitic enzyme over the human host enzyme. The results presented here underscore the need for identifying high affinity scaffolds that are able to discriminate between the target in host and pathogen. At the same time, this study offers insight about the enzyme active site for further exploration of the chemical space. Although the docking technique we used quite reliably predicts the binding conformation of ligands, our results point out the need to account for ligand induced conformational changes in the DHFR structure for more accurate prediction of protein–ligand interactions.

Despite the high degree of overall homology in primary sequences and in three-dimensional structures of DHFR from different organisms, DHFR remains a potentially attractive target for drugs to treat microbial infection. For example, trimethoprim exhibits a 10^5-fold selectivity for bacterial DHFR as compared to vertebrate enzymes. Probing the active sites of both the host and pathogen enzyme with diverse scaffolds will lead to the identification of hot spots for selectivity.

4. Experimental

### 4.1. General methods for synthesis

Solvent evaporations were carried out in vacuo with a rotary evaporator. Thin layer chromatography (TLC) was performed on silica gel plates with fluorescent indicator (Whatmann, silica gel, UV254, 25 μm plates). Spots were visualized by UV light (254 and 365 nm). Purification by column and flash chromatography was carried out using 'BAKER' silica gel (40 μm) in the solvent systems indicated. The amount (weight) of silica gel for column chromatography was in the range of 50–100 times the amount (weight) of the crude compounds being separated. Proton nuclear magnetic resonance (^{1}H NMR) and carbon nuclear magnetic resonance (^{13}C NMR) spectra were recorded on a Bruker DPX-300 spectrometer using TMS as internal standard. The values of chemical shifts (δ) are given in ppm and coupling constants (J) in hertz. The chemical shift values are reported as parts per million (ppm) relative to tetramethylsilane as internal standard. Mass spectra were recorded on Micromass Platform LCC instrument. Anhydrous solvents used for reactions were purchased in Sure-Seal™ bottles from Aldrich Chemical Company. Other reagents were purchased from Aldrich, Lancaster or Fisher chemical companies and used as received.

4.2. Syntheses

The chemical structures of all target compounds including TMQ for comparison are shown in Figure 1.

Synthesis of target compounds **6a–d** is outlined in Scheme 1. The synthesis started with commercially available 2-fluoro-5-formylbenzonitrile (**1**). The 2-fluoro-5-formylbenzonitrile **1** was aminated with 5-amino-2-methoxyphenol **2** in presence of NaC-NBH$_3$ and ZnCl$_2$ in methanolic medium to afford the aminated product **3** in 77% yield. The alkylation of hydroxy compound **3** with alkyl halides in the presence of NaH in anhydrous DMF gave the compounds **4a–d** in 81–90% yield. The target compounds, **6a–d**, were prepared from the compounds **4a–d** in 44–83% yield by refluxing with guanidine carbonate (**5**) in *N,N*-dimethylacetamide.

Synthesis of target compound **8** is outlined in Scheme 2. Reductive N-alkylation of compound **4c** with propionaldehyde using NaCNBH$_3$ and few drops of conc. HCl afforded the *N*-propyl compound **7** in 93% of yield. Compound **7** was then converted to the target quinazoline **8** in 38% yield by refluxing with guanidine carbonate **5** in *N,N*-dimethylacetamide.
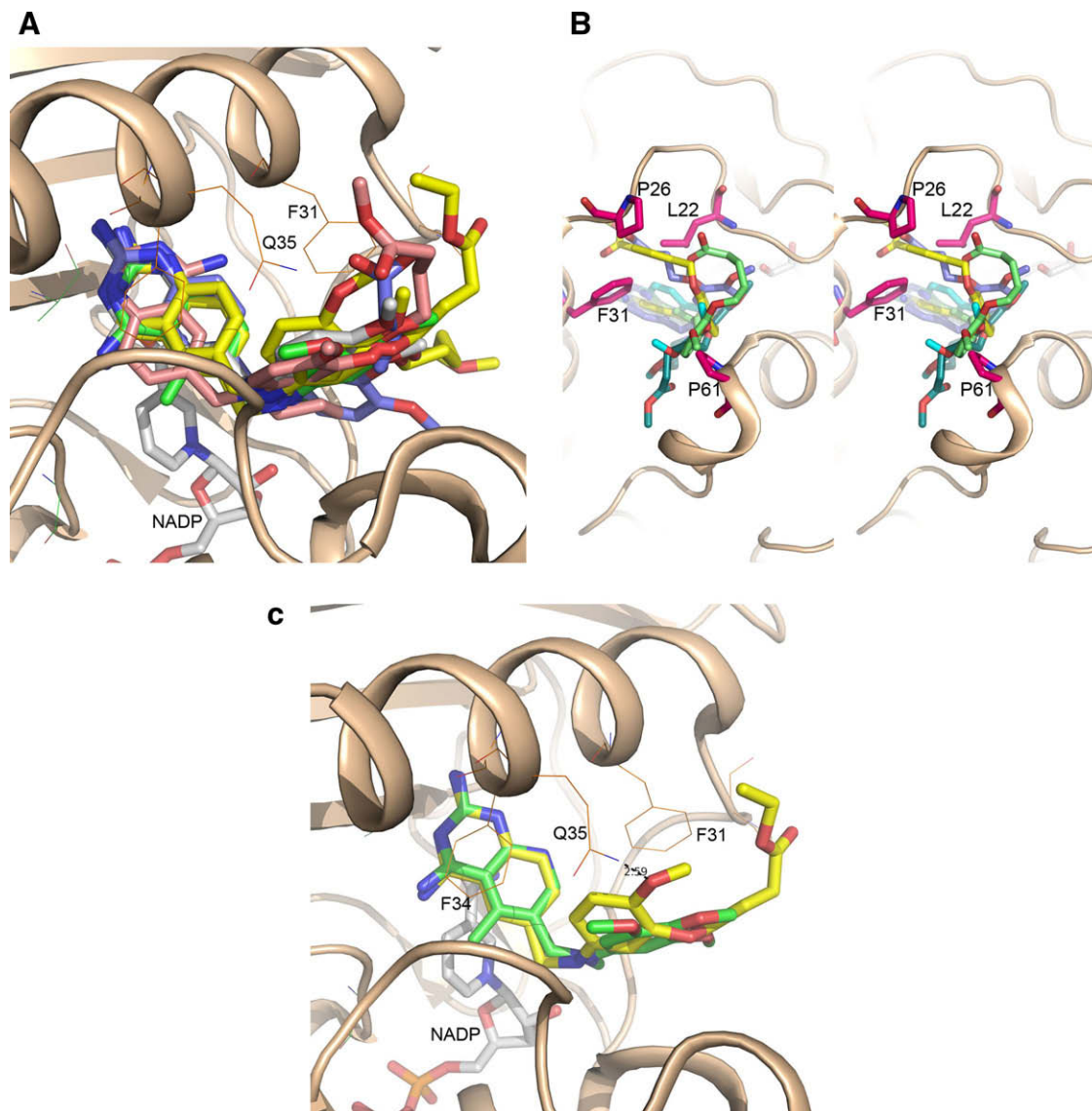
Figure 7. Docking of the inhibitors into the active site of hDHFR. (A) Docked poses of inhibitors in hDHFR active site. Protein model is shown in cartoon representation. Ligands and NADP are shown as stick models. Selected residues (Phe31, Phe 34, and Gln 35) are shown in line representation. (B) Stereoscopic view showing docked poses of several inhibitors as stick models as placed in the *Tc*DHFR active site superimposed onto the hDHFR structure (shown as cartoon). Residues Pro26, Phe31, and Pro61 in hDHFR close to the inhibitors are shown as stick models (color code: pink-C, blue-N, red-O). (C) Binding of inhibitor **6b** in the hDHFR active site. The protein is shown as a cartoon diagram. Docked conformation of **6b** is shown as stick model (color code: yellow-C, blue-N, red-O). For comparison, the compound CO4 is shown as stick model (color code: green-C, blue-N, red-O). NADP is also shown as stick model (color code: white-C, blue-N, red-O). Amino acid residues Phe31, Phe34, and Gln35 shown in line representation are labeled. Gln35 side chain N atom is within hydrogen bonding distance from the methoxy oxygen atom on the ligand.

The carboxylic acid derivative **9** is prepared by hydrolysis of corresponding ethyl ester **6b** using 1 N. NaOH in THF with 72% yield (Scheme 3).

4.2.1. 5-[(3-Hydroxy-4-methoxyphenylamino)methyl]-2-fluorobenzonitrile (3)

To a solution of 2-fluoro-5-formylbenzonitrile **1** (4.05 g, 27.1 mmol) in anhydrous MeOH (85 mL) 5-amino-2-methoxyphenol **2** (4.16 g, 29.9 mmol) was added and stirred at room temperature for 15 min. A solution of NaCNBH$_3$ (1.88 g, 29.9 mmol) and ZnCl$_2$ (1.85 g, 13.6 mmol) in MeOH (60 mL) was added dropwise to the reaction mixture and stirred at room temperature for 12 h. After completing the reaction (as indicated by tlc), water (2 mL) was added to quench the reaction mixture and solvent was completely removed under reduced pressure. The residue obtained was dissolved in dichloromethane (60 mL) and washed with water (3 × 30 mL), brine (1 × 30 mL) and dried over Na$_2$SO$_4$. The drying agent was filtered off and the solvent was concentrated in vacuum

to obtain the crude product. The crude product was purified by flash chromatography on silica gel using EtOAc–hexanes (1:3) as the eluent to afford the pure 5-[(3-hydroxy-4-methoxyphenyl-amino)methyl]-2-fluorobenzonitrile **3** (5.67 g, 77%); mp 113 °C; ^{1}H NMR (CDCl$_3$) δ 3.81 (s, 3H), 3.95 (br s, 1H), 4.30 (s, 2H), 5.61 (br s, 1H), 6.04 (dd, 1H, J_1 = 2.7 Hz, J_2 = 8.6 Hz), 6.23 (d, 1H, J = 2.7 Hz), 6.70 (d, 1H, J = 8.6 Hz), 7.18 (t, 1H, J = 8.5 Hz) and 7.52–7.65 (m, 2H); ^{13}C NMR (CDCl$_3$) δ 47.5, 56.9, 101.0, 101.4 and 101.5 (C–F coupling), 104.1, 112.6, 114.2, 116.6 and 116.8 (C–F coupling), 131.9, 133.9 and 134.0 (C–F coupling), 137.2 and 137.3 (C–F coupling), 139.7, 142.5, 146.8, 161.0 and 163.6 (C–F coupling); MS (ES$^+$): m/z = 273 [M+H].

4.2.2. General procedures for the preparation of 4

To a solution of compound **3** (2.47 g, 9.1 mmol) in anhydrous DMF (4 mL), NaH (0.261 g, 10.9 mmol) was added and stirred at room temperature for 30 min. Ethyl 4-bromobutyrate (1.44 mL, 10 mmol) was added to the reaction mixture and stirred at room

Table 4
Distribution of total energy of ligand–receptor interactions based on docked poses of inhibitors in the *Tc*DHFR or hDHFR active site

	Total (kcal/mol)	van der Waals (kcal/mol)	Hydrogen bond (kcal/mol)
TcDHFR			
6a	−12.07	−9.45	−2.46
6b	−11.92 (−11.58)[a]	−10.41 (−11.29)	−2.29 (−1.76)
6c	−12.43	−10.45	−2.42
6d	−12.21	−10.00	−2.22
8	−8.36	−8.91	−0.46
9	−9.13	−9.14	−0.79
TMQ	−10.09 (−9.72)	−10.16 (−9.64)	−2.34 (−0.89)
hDHFR			
6a	−11.32	−10.09	−2.39
6b	−13.33	−11.43	−2.61
6c	−12.55	−11.03	−1.33
6d	−11.59	−9.47	−1.05
8	−12.92	−11.07	−1.19
9	−13.48	−10.96	−2.26
CO4	−13.52 (−11.71)	−10.05 (−10.94)	−2.88 (−1.12)

Based on results from PEARLS web server (http://ang.cz3.nus.edu.sg/cgi-bin/prog/rune.pl).[26]

[a] Values in parenthesis are based on X-ray crystal structures of enzyme:cofactor:inhibitor complex.

temperature for 12 h. After completion of the reaction (as indicated by tlc), the reaction mixture was diluted with water (60 mL) and extracted with EtOAc (3 × 75 mL). The combined organic layer was washed with water (3 × 75 mL) and brine (1 × 75 mL). The extract was then dried over Na_2SO_4. After the removal of the drying agent, solvent was completely removed to obtain the crude product which was purified by flash chromatography on silica gel using EtOAc–hexanes (1:3) as the eluent to afford pure products **4a–d**.

4.2.2.1. 5-{[(3,4-Dimethoxyphenyl)amino]methyl}-2-fluorobenzonitrile (4a). Isolated as a yellow oil; (83%); ^{1}H NMR (CDCl$_3$) δ 3.80 (s, 3H), 3.82 (s, 3H), 4.32 (s, 2H), 6.06 (dd, 1H, J_1 = 2.7 Hz, J_2 = 8.5 Hz), 6.24 (d, 1H, J = 2.7 Hz), 6.72 (d, 1H, J = 8.5 Hz), 7.19 (t, 1H, J = 8.5 Hz), 7.60–7.66 (m, 2H); ^{13}C NMR (CDCl$_3$) δ 48.0, 56.2, 57.0, 99.6, 101.7 and 101.8 (C–F coupling), 103.9, 113.4, 114.4, 116.9, 117.1, 132.3, 134.2, 134.3 (C–F coupling), 137.4, 137.5 (C–F coupling), 142.4, 142.5 (C–F coupling), 150.4, 161.4, 163.9 (C–F coupling); MS (ES[+]): m/z = 287 [M+H].

4.2.2.2. Ethyl 4-[5-(3-cyano-4-fluorobenzylamino)-2-methoxyphenoxy]butanoate (4b). Isolated as a yellow oil; (81%); ^{1}H NMR (CDCl$_3$) δ 1.25 (t, 3H, J = 7.6 Hz), 2.06–2.15 (m, 2H), 2.51 (t, 2H, J = 7.2 Hz); 3.76 (s, 3H), 3.98 (t, 2H, J = 6.4 Hz), 4.13 (q, 2H, J = 7.6 Hz), 4.30 (s, 2H), 6.06 (dd, 1H, J_1 = 2.8 Hz, J_2 = 8.4 Hz), 6.26 (d, 1H, J = 2.8 Hz), 6.71 (d, 1H, J = 8.4 Hz), 7.17 (t, 1H, J = 8.4 Hz), 7.56–7.67 (m, 2H); ^{13}C NMR (CDCl$_3$) δ 14.3, 24.5, 30.8, 47.6, 57.0, 60.5, 67.9, 101.0, 101.4 and 101.5 (C–F coupling), 104.2, 114.1, 116.5 and 116.7 (C–F coupling), 132.0, 133.9 and
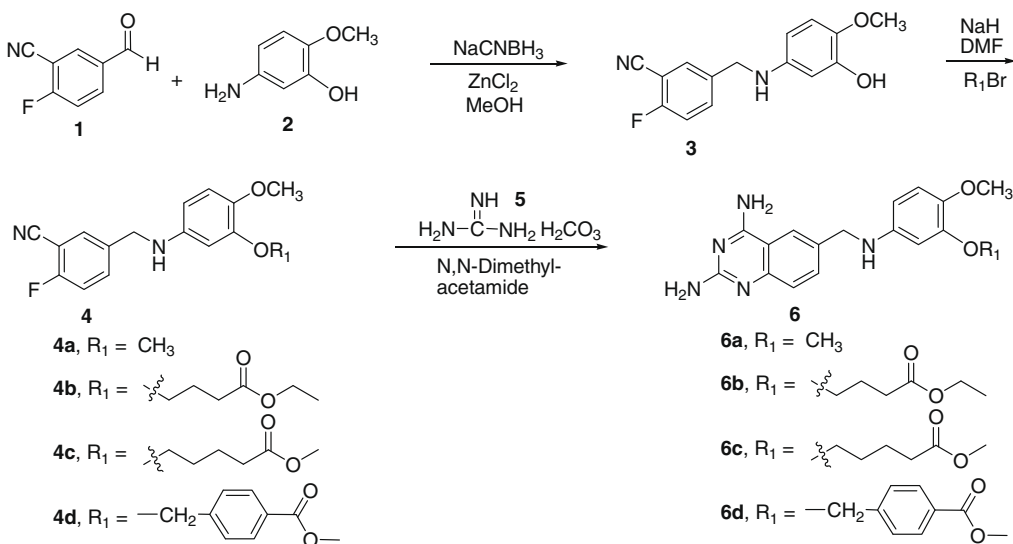
Scheme 1.
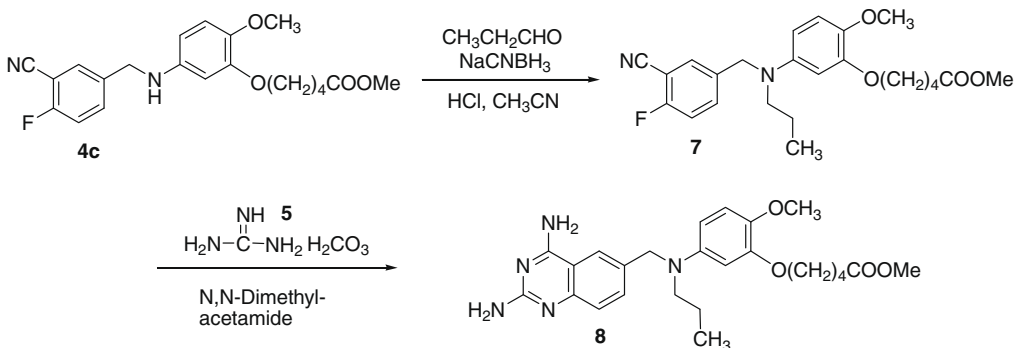
Scheme 2.
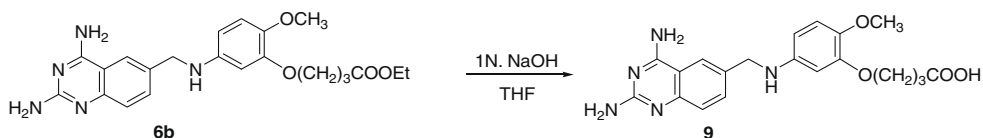
Scheme 3.

134.0 (C–F coupling), 137.2 (2C, C–F coupling), 142.2, 142.5, 149.5, 161.0 and 163.5 (C–F coupling), 173.3; MS (ES⁺): m/z = 387 [M+H].

4.2.2.3. Methyl 4-[5-(3-cyano-4-fluorobenzylamino)-2-methoxy-phenoxy]pentanoate (4c). Isolated as a yellow oil; (90%); ¹H NMR (CDCl₃) δ 1.81–1.86 (m, 4H), 2.41 (t, 2H, J = 6.8 Hz), 3.68 (s, 3H), 3.79 (s, 3H), 3.96 (t, 2H, J = 6.8 Hz), 4.32 (s, 2H), 6.08 (dd, 1H, J₁ = 2.7 Hz, J₂ = 8.5 Hz), 6.24 (d, 1H, J = 2.7 Hz), 6.73 (d, 1H, J = 8.5 Hz), 7.20 (t, 1H, J = 8.5 Hz), 7.60–7.66 (m, 2H); ¹³C NMR (CDCl₃) δ 21.9, 29.0, 34.1, 48.0, 52.0, 57.4, 68.8, 101.2, 101.8, 102.0 (C–F coupling), 104.4, 114.4, 116.9, 117.1 (C–F coupling), 132.3, 134.2, 134.3 (C–F coupling), 137.5 (2C, C–F coupling), 142.5, 142.9, 150.0, 161.4, 163.9 (C–F coupling), 174.3; MS (ES⁺): m/z = 387 [M+H].

4.2.2.4. Methyl 4-({5-[(3-cyano-4-fluorobenzyl)amino]-2-methoxy-phenoxy}methyl)benzoate (4d). Isolated as a yellow oil; (86%); ¹H NMR (CDCl₃) δ 3.81 (s, 3H), 3.91 (s, 3H), 4.02 (br s, 1H), 4.21 (s, 2H), 5.12 (s, 2H), 6.06–6.17 (m, 2H), 6.76 (d, 1H, J = 8.4 Hz), 7.11 (t, 1H, J = 8.7 Hz), 7.44 (d, 2H, J = 8.4 Hz), 7.46–7.57 (m, 2H), 7.96–8.04 (m, 2H); ¹³C NMR (CDCl₃) δ 47.4, 52.1, 57.0, 70.5, 101.3 and 101.5 (C–F coupling), 101.7, 105.1, 114.0, 114.3, 116.4 and 116.6 (C–F coupling), 126.6, 129.5, 129.8, 131.7, 133.6 and 133.7 (C–F coupling), 137.0 (2C, C–F coupling), 142.1, 142.5, 142.6 (2C, C–F coupling), 149.0, 160.4 and 163.9 (C–F coupling), 166.8; MS (ES⁺) m/z 421 (M+H).

4.2.3. General procedures for the preparation of 6a–d

To the solution of compound **4** (7 mmol) in anhydrous N,N-dimethylacetamide (25 mL), guanidine carbonate (1.26 g, 7 mmol) was added and the resulting mixture was heated at 140 °C for 5 h. The solvent was completely removed under vacuum and the residue obtained was purified by flash column chromatography over silica gel using MeOH–NH₃ saturated CHCl₃ (1:9) to furnish the pure products **6a–d**.

4.2.3.1. 6-[(3,4-Dimethoxyanilino)methyl]-2,4-quinazolinedi-amine (6a). Isolated as a yellow oil; (83%); ¹H NMR (DMSO-d₆) δ 3.59 (s, 3H, 3.65 (s, 3H), 4.16 (d, 1H, J = 5.5 Hz), 5.72 (br t, 1H, J = 5.5 Hz), 6.01 (br s, 2H), 6.07 (dd, 1H, J₁ = 2.5 Hz, J₂ = 8.6 Hz), 6.34 (d, 1H, J = 2.5 Hz), 6.65 (d, 1H, J = 8.6 Hz), 7.16 (d, 1H, J = 8.6 Hz), 7.30 (br s, 2H), 7.51 (dd, 1H, J₁ = 1.8 Hz, J₂ = 8.6 Hz); ¹³C NMR (DMSO-d₆) δ 47.7, 55.2, 56.6, 99.0, 102.8, 109.8, 114.3, 122.5, 123.9, 131.9, 132.5, 140.2, 143.9, 149.8, 160.3, 162.4; MS (ES⁺): m/z = 326 [M+H].

4.2.3.2. Ethyl 4-(5-[(2,4-diamino-6-quinazolinyl)methyl]amino-2-methoxyphenoxy) butanoate (6b). Isolated as a yellow solid; (44%); mp 194 °C; ¹H NMR (DMSO-d₆) δ 1.17 (t, 3H, J = 7.1 Hz), 1.86–1.97 (m, 2H), 2.43 (t, 2H, J = 7.3), 3.60 (s, 3H), 3.86 (t, 2H, J = 6.3 Hz), 4.04 (q, 2H, J = 7.1 Hz), 4.15 (d, 2H, J = 5.1 Hz), 5.69 (t, 1H, J = 5.1 Hz), 6.04 (br s, 2H), 6.09 (dd, 1H, J₁ = 2.4 Hz, J₂ = 8.6 Hz), 6.33 (d, 1H, J = 2.4 Hz), 6.68 (d, 1H, J = 8.6 Hz), 7.17 (d, 1H, J = 8.6 Hz), 7.30 (br s, 2H), 7.50 (dd, 1H, J₁ = 1.6 Hz, J₂ = 8.6 Hz), 7.99 (s, 1H); ¹³C NMR (DMSO-d₆) δ 14.1, 24.4, 30.1, 47.7, 56.7, 59.9, 67.0, 100.2, 103.3, 109.9, 114.7, 122.4, 124.1, 131.8, 132.5, 140.5, 144.0, 149.0, 151.3, 160.4, 162.4, 172.6; MS (ES⁺): m/z = 426 [M+H].

4.2.3.3. Methyl 5-(5-[(2,4-diamino-6-quinazolinyl)methyl]amino-2-methoxyphenoxy) pentanoate (6c). Isolated as a yellow oil; (48%); ¹H NMR (DMSO-d₆) δ 1.61–1.66 (m, 4H), 2.35 (t, 2H, J = 6.1 Hz), 3.57 (s, 3H), 3.59 (s, 3H), 3.82 (t, 2H, J = 6.1 Hz), 4.20 (s, 2H), 5.75 (br s, 1H), 6.05 (dd, 1H, J₁ = 2.7 Hz, J₂ = 8.7 Hz), 6.31 (d, 1H, J = 2.7 Hz), 6.66 (d, 1H, J = 8.7 Hz), 6.91 (br s, 2H), 7.28 (d, 1H, J = 8.4 Hz), 7.63 (d, 1H, J = 8.4 Hz), 8.09 (br s, 2H), 8.15 (s, 1H); ¹³C NMR (DMSO-d₆) δ 22.3, 29.2, 34.6, 48.5, 57.5, 68.4, 101.0, 103.9, 110.6, 115.5, 123.4, 124.0, 133.1, 133.6, 141.3, 144.8, 150.0, 150.7, 160.8, 160.78, 163.3, 175.9; MS (ES⁺): m/z = 426 [M+H].

4.2.3.4. Methyl 4-[(5-[(2,4-diamino-6-quinazolinyl)methyl]amino-2-methoxyphenoxy) methyl]benzene carboxylate (6d). Isolated as an oil; (54%); ¹H NMR (DMSO-d₆) δ 3.63 (s, 3H), 3.85 (s, 3H), 4.17 (br s, 2H), 5.07 (s, 2H), 5.81 (br s, 1H), 6.12 (dd, 1H, J₁ = 8.4 Hz, J₂ = 2.3 Hz), 6.34–6.44 (m, 1H), 6.62–6.86 (m, 3H), 7.24 (d, 1H, J = 8.4 Hz), 7.42–7.68 (m, 3H), 7.81–8.04 (m, 4H), 8.09–8.24 (m, 1H); ¹³C NMR (DMSO-d₆) δ 47.9, 52.6, 57.3, 69.7, 101.2, 104.7, 110.0, 115.5, 121.6, 123.3, 127.8, 129.3, 129.7, 133.8, 134.2, 141.2, 143.5, 144.2, 146.5, 149.1, 158.6, 163.1, 166.5; MS (ES⁺) m/z 460 (M+H).

4.2.4. Preparation of methyl 5-{5-[(3-cyano-4-fluorobenzyl)(propyl)amino]-2-methoxyphenoxy}pentanoate (7)

To a stirred solution of methyl 4-[5-(3-cyano-4-fluorobenzyl-amino)-2-methoxyphenoxy] pentanoate **4c** (0.055 g, 0.142 mmol) in CH₃CN (10 mL) was added propionaldehyde (0.017 g, 0.28 mmol) followed by NaCNBH₃ (0.027 g, 0.43 mmol). It remained as a suspension. The pH of the suspension was adjusted to 2–3 by drop wise addition of concentrated HCl. As the mixture was acidified, the suspended starting material began to dissolve into solution, followed by precipitation of the crude product. The suspension containing the crude product was stirred at room temperature for an additional 0.5 h. The crude product was filtered, stirred with 2 N Na₂CO₃ and washed with water, brine and dried with Na₂SO₄ and concentrated in vacuo. The residue was purified by column chromatography using silica gel with hexane–EtOAc (85:15) as eluent to obtain the pure product **7** as a yellow oil (0.057 g, 93%); ¹H NMR (CDCl₃) δ 0.94 (t, 3H, J = 7.3 Hz), 1.61–1.67 (m, 2H), 1.79–1.83 (m, 4H), 2.40 (t, 2H, J = 6.7 Hz), 3.26 (t, 2H, J = 7.3 Hz), 3.68 (s, 3H), 3.79 (s, 3H), 3.95 (t, 2H, J = 6.7 Hz), 4.43 (s, 2H), 6.19 (dd, 1H, J₁ = 2.5 Hz, J₂ = 8.6 Hz), 6.30 (d, 1H, J = 2.5 Hz), 6.76 (d, 1H, J = 8.8 Hz), 7.16 (t, 1H, J = 8.6 Hz), 7.47–7.52 (m, 2H); ¹³C NMR (CDCl₃) δ 12.0, 20.9, 22.0, 29.1, 34.1, 52.0, 54.7, 55.0, 57.3, 69.0, 101.7, 101.9 (C–F coupling), 102.1, 106.3, 114.4, 114.5, 116.8, 117.0 (C–F coupling), 132.0, 133.8, 133.9 (C–F coupling), 137.2, (2C, C–F coupling), 142.6, 143.7, 149.8, 161.2, 163.8 (C–F coupling), 174.3; MS (ES⁺): m/z = 429 [M+H].

4.2.5. Preparation of methyl 5-{5-[[(2,4-diamino-6-quinazolinyl)methyl](propyl)amino]-2-methoxyphenoxy} pentanoate (8)

Compond **8** was synthesized from **7** (0.1 g, 0.23 mmol) and guanidine carbonate (0.063 g, 0.35 mmol) in N,N-dimehtylacetamide (5 mL) according to the procedure described for **6**. Isolated as a yellow oil (0.041 g, 38%); ¹H NMR (DMSO-d₆) δ 0.87 (t, 3H, J = 7.3 Hz), 1.53–1.63 (m, 6H), 2.33 (t, 2H, J = 6.7 Hz), 3.17 (s, 2H), 3.58 (s, 3H), 3.61 (s, 3H), 3.84 (br t, 2H), 4.14 (br s, 1H), 4.42 (s, 2H), 6.20 (dd,

1H, J_1 = 2.6 Hz, J_2 = 8.8 Hz), 6.35–6.38 (m, 3H), 6.73 (d, 1H, J = 8.8 Hz), 7.19 (d, 1H, J = 8.5 Hz), 7.42 (d, 1H, J = 8.5 Hz), 7.64 (br s, 2H), 7.95 (s, 1H); ^{13}C NMR (DMSO-d_6) δ 12.3, 20.6, 22.1, 29.0, 33.7, 49.5, 52.1, 57.4, 68.5, 80.0, 101.8, 105.8, 110.6, 115.4, 122.1, 122.9, 128.3, 127.2, 133.2, 141.5, 144.5, 149.8, 163.3, 174.1; MS (ES$^+$): m/z = 468 [M+H].

4.2.6. Preparation of 4-(5-[(2,4-diamino-6-quinazolinyl) methyl]amino-2-methoxyphenoxy) butanoic acid (9)

To a stirred solution of ethyl 4-(5-[(2,4-diamino-6-quinazolinyl)methyl]amino-2-methoxy phenoxy)butanoate (**6b**) (0.1 g, 0.23 mmol) in THF (5 mL) and MeOH (2 mL) was added 1 N. NaOH solution (2.5 mL) at room temparature for 4 h. Then it was acidified with 1 N HCl and solvent was completely removed under reduced pressure. The residue obtained was dissolved in dichloromethane (25 mL) and washed with water (3 × 15 mL), brine (1 × 15 mL) and dried over Na$_2$SO$_4$. The drying agent was removed and the solvent was concentrated in vacuum to obtain the crude product. The crude product was purified by flash chromatography on silica gel using CHCl$_3$–methanol (9:1) as the eluent to give 4-(5-[(2,4-diamino-6-quinazolinyl)methyl]amino-2-methoxy phenoxy)butanoic acid (**9**) (0.067 g, 72%) as a yellow oil; ^{1}H NMR (DMSO-d_6) δ 1.88 (q, 2H, J = 6.5 Hz), 2.32 (t, 2H, J = 6.5 Hz), 3.59 (s, 3H), 3.85 (t, 2H, J = 6.5 Hz), 4.16 (s, 2H), 6.04 (br s, 1H), 6.05 (d, 1H, J = 7.7 Hz), 6.33 (s, 1H), 6.66 (d, 1H, J = 8.5 Hz), 6.92 (br s, 2H), 7.21–7.24 (m, 1H), 7.58 (d, 1H, J = 7.7 Hz), 7.84 (br s, 2H), 8.07 (s, 1H); ^{13}C NMR (DMSO-d_6) δ 24.5, 30.4, 47.5, 56.7, 67.1, 100.2, 103.2, 109.2, 109.6, 114.7, 122.7, 133.2, 140.6, 143.8, 149.1, 162.6, 174.5; MS (ES$^+$): m/z = 398[M+H].

4.3. Enzyme inhibitory assay

Recombinant bifuntional enzyme (*Tc*DHFR–TS) was used throughout this study. Inhibitory activity of the reported compounds was measured in a spectrophotometric assay using the bifunctional enzyme as described previously.[6] Briefly, the reaction mixture for *Tc*DHFR contained 1 ml of 50 mM Tris–HCl buffer, pH 7.0, dihydrofolic acid (DHF), 100 μM NADPH and 0.5–1.0 μg of enzyme, and the reaction velocity was measured by monitoring absorbance at 340 nm for 30 s at 22.6 °C. Human DHFR (hDHFR) activity was measured in 50 mM KH$_2$PO$_4$ buffer, pH 7.3, containing 250 mM KCl and 5 mM 2-mercaptoethanol. The IC$_{50}$ value (concentration of inhibitor required for 50% inhibition) of each inhibitor was determined by measuring reaction velocity at several inhibitor concentrations for two (hDHFR) or three (*Tc*DHFR) different DHF concentrations, and then averaged. All measurements were conducted in triplicate. The reproducibility and stability of the compound assays were verified by repeating the assays on different days.

In general, K_i values for each inhibitor were calculated from the corresponding IC$_{50}$ values. The formulas used for calculation of IC$_{50}$ and K_i values from the observed experimental reaction rates are shown in Table 1. However, in order to judge the accuracy of this calculation we experimentally determined K_i values for compounds **6a** and **6b** (for *Tc*DHFR) for comparison with calculated values. For these measurements reaction velocities were obtained using five different concentrations of DHF at three different inhibitor concentrations. The experimental K_i values were determined from Lineweaver–Burk plots using the 'Enzyme Kinetics' module in SigmaPlot (Systat Software Inc.).

4.4. Crystallization of ternary complex with 6b, intensity data collection, structure solution

Attempts were made to crystallize ternary (inhibitor:cofactor:enzyme) complexes of **6a** and **6b** using the bifunctional enzyme. However, diffraction quality crystals were obtained only with **6b**. Complex of **6b** with *T. cruzi* enzyme was obtained by incubating bifunctional *Tc*DHFR–TS enzyme (10 mg/ml) with 1 mM NADP, 1 mM dUMP and 1 mM inhibitor for 3 h at 4 °C. Crystals were grown from 50 mM HEPES, pH 7.0, 10 mM magnesium chloride and 5–10% ethylene glycol (EDO) using 1.5–1.7 M ammonium sulfate as precipitant. Crystals appeared in 2–3 days and reached their maximum size (0.2 × 0.2 × 0.15 mm) in two weeks. These crystals belong to tetragonal space group P4$_3$2$_1$2 with four molecules in the asymmetric unit. For cryo-protection we used 30% EDO in the mother liquor. Intensity data for the complex were collected at the Advanced Photon Source (APS) synchrotron IMCA 17ID beam line and were processed using HKL2000 and D*TREK program packages.[19,20]

The crystal structure was solved by molecular replacement with the structure of one molecule of ligand-free *Tc*DHFR–TS (PDB Id: 2H2Q) as search model using the program PHASER.[21] Difference electron density maps allowed the placement of cofactor and inhibitor in all four subunits (A, B, C, and D) of the inhibitor complex. Several atoms in the ethylbutanoate chain were disordered and the occupancy of these atoms was kept at zero. No density for the dUMP molecule was observed and instead one sulfate ion (from the crystallization medium) was located at the position normally occupied by the phosphate group of dUMP. Several rounds of map fitting and structure refinement were carried out with programs COOT[22] and REFMAC5.[23]

4.5. Molecular docking and energy analysis

Ligand structures generated with the program package Marvin-Beans/JChem (ChemAxon; see: http://www.chemaxon.com/) provided the input files for docking into the active sites of *Tc*DHFR and hDHFR using the program iGemDock.[24,25] The program includes routines for target and database preparation, molecular docking, and post-docking analysis. The active site of PDB entry 3CLB (*Tc*DHFR–TS in complex with NADP and TMQ) was used for docking of the inhibitors in case of *Tc*DHFR. The ligand binding area was defined by including the cofactor and all protein residues within 8 Å distance from the ligand (TMQ). Atom formal charges and atom types are then added. During docking the protein was kept rigid since the docking program does not allow the inclusion of flexibility of protein residues or defined side chain rotamers. On the other hand the docking procedure executes flexible docking for each ligand in the ligand database. For scoring we used the Gemdock scoring function that consists of a simple empirical scoring function and a pharmacophore-based scoring function (includes electrostatic, steric, and hydrogen bonding potentials), which is described in the literature.[24,25] In a final step, iGemDock re-ranks and sorts all docked ligand conformations that can be displayed in the post-docking analysis.

Docked poses of TMQ and **6b** in *Tc*DHFR were compared with the experimental binding modes in the crystal structure (3HBB and 3KJS, respectively). In the absence of a crystal structure of hDHFR with TMQ we used the structure of hDHFR with an analog of TMQ (PDBID: 1PD8). The docked poses that provided the closest structural alignment of the 2,4-diaminoquinazoline ring of each inhibitor with the same moiety in TMQ, **6b** or CO4 were considered as most likely binding modes.

We also calculated estimated binding affinities based on docked poses of all six compounds for *Tc*DHFR and hDHFR using the PEARLS web server (http://ang.cz3.nus.edu.sg/cgi-bin/prog/rune.pl)[26] and compared these with data obtained for the X-ray poses of TMQ, **6b**, and CO4 (Table 3). An energy analysis for this set of compounds shows the contribution of van der Waals and hydrogen bond energy to the total free energy (Table 4). Figures have been prepared using PyMOL.[27]

Acknowledgments

References and notes

1. Moncayo, A.; Silveira, A. C. *Mem. Inst. Oswaldo Cruz* **2009**, *104*, 17.
2. Ferone, R.. In *Antimalarial Drugs*; Peter, W., Richards, W. H. G., Eds.; Springer: New York, 1984; Vol. 68, pp 207–221.
3. Olliari, P. L.; Yuthavong, Y. *Pharmacol. Ther.* **1999**, *81*, 91.
4. Chan, D. C. M.; Anderson, A. C. *Curr. Med. Chem.* **2006**, *13*, 377.
5. Yuthavong, Y.; Yuvaniyama, J.; Chitnumsub, P.; Vanichtanankul, J.; Chusacultanachai, S.; Tarnchompoo, B.; Vilaivan, T.; Kamchonwongpaisan, S. *Parasitology* **2005**, *130*, 249.
6. Senkovich, O.; Bhatia, V.; Garg, N.; Chattopadhyay, D. *Antimicrob. Agents Chemother.* **2005**, *49*, 3234.
7. Senkovich, O.; Schormann, N.; Chattopadhyay, D. *Acta Crystallogr. D Biol. Crystallogr.* **2009**, *65*, 704.
8. Schormann, N.; Senkovich, O.; Walker, K.; Wright, D. L.; Anderson, A. C.; Rosowsky, A.; Ananthan, S.; Shinkre, B.; Velu, S.; Chattopadhyay, D. *Proteins* **2008**, *73*, 889.
9. Davoll, J.; Johnson, A. M.; Davies, H. J.; Bird, O. D.; Clarke, J.; Elslager, E. F. *J. Med. Chem.* **1972**, *15*, 812.
10. Gilbert, I. H. *Biochim. Biophys. Acta* **2002**, *1587*, 249.
11. Zuccotto, F.; Zvelebil, M.; Brun, R.; Chowdhury, S. F.; Di Lucrezia, R.; Leal, I.; Maes, L.; Ruiz-Perez, L. M.; Gonzalez Pacanowska, D.; Gilbert, I. H. *Eur. J. Med. Chem.* **2001**, *36*, 395.
12. Zuccotto, F.; Brun, R.; Gonzalez Pacanowska, D.; Ruiz Perez, L. M.; Gilbert, I. H. *Bioorg. Med. Chem. Lett.* **1999**, *9*, 1463.
13. Chowdhury, S. F.; Villamor, V. B.; Guerrero, R. H.; Leal, I.; Brun, R.; Croft, S. L.; Goodman, J. M.; Maes, L.; Ruiz-Perez, L. M.; Pacanowska, D. G.; Gilbert, I. H. *J. Med. Chem.* **1999**, *42*, 4300.
14. Anderson, A. C. *Acta Crystallogr. F Struct. Biol. Cryst. Commun.* **2005**, *61*, 258.
15. Pan, H.; Lee, J. C.; Hilser, V. J. *Proc. Natl. Acad. Sci. U.S.A.* **2000**, *97*, 12020.
16. Schnell, J. R.; Dyson, H. J.; Wright, P. E. *Ann. Rev. Biophys. Biomol. Struct.* **2004**, *33*, 119.
17. Matthews, D. A.; Bolin, J. A.; Burridge, J. M.; Filman, D. J.; Volz, K. W.; Kaufman, B. T.; Beddell, C. R.; Champness, J. N.; Stammers, D. K.; Kraut, J. *J. Biol. Chem.* **1985**, *260*, 381.
18. Cody, V.; Luft, J. R.; Pangborn, W.; Gangjee, A. *Acta Crystallogr. D Biol. Crystallogr.* **2003**, *59*, 1603.
19. Otwinowski, Z.; Minor, W. *Methods Enzymol.* **1997**, *276*, 307.
20. Pflugrath, J. W. *Acta Crystallogr. D Biol. Crystallogr.* **1999**, *55*, 1718.
21. McCoy, A. J.; Grosse-Kunstleve, R. W.; Adams, P. D.; Winn, M. D.; Storoni, L. C.; Read, R. J. *J. Appl. Crystallogr.* **2007**, *40*, 658.
22. Emsley, P.; Cowtan, K. *Acta Crystallogr. D Biol. Crystallogr.* **2004**, *60*, 2126.
23. Murshudov, G. N.; Vagin, A. A.; Dodson, E. J. *Acta Crystallogr. D Biol. Crystallogr.* **1997**, *53*, 240.
24. Yang, J.-M.; Chen, C. C. *Proteins* **2004**, *55*, 288.
25. Yang, J.-M. *J. Comput. Chem.* **2004**, *25*, 843.
26. Han, L. Y.; Lin, H. H.; Li, Z. R.; Zheng, C. J.; Cao, Z. W.; Xie, B.; Chen, Y. Z. *J. Chem. Inf. Model.* **2006**, *46*, 445.
27. DeLano, W. L. *DeLano Scientific*; San Carlos: CA, 2002.
28. Reche, P.; Arrebola, R.; Olmo, A.; Santi, D. V.; Gonzalez-Pacanowska, D.; Ruiz-Perez, L. M. *Mol. Biochem. Parasitol.* **1994**, *65*, 247.
29. White, E. L.; Ross, L. J.; Cunningham, A.; Escuyer, V. F. E. M. S. *Microbiol. Lett.* **2004**, *232*, 101.